

1 Water-soluble iron emitted from vehicle exhaust is linked to primary speciated organic
2 compounds

3
4 Joseph R. Salazar*, Benton T. Cartledge*, John P. Haynes*, Rachel York-Marini*, Allen L
5 Robinson‡, Greg T. Drozd[€], Allen H. Goldstein[¥], Sirine C. Fakra[¢], Brian J. Majestic*

6 *University of Denver, Department of Chemistry and Biochemistry

7 ‡Carnegie Mellon University, College of Engineering

8 ¥University of California, Berkeley Department of Civil and Environmental Engineering

9 €Colby College Department of Chemistry

10 ¢Advanced Light Source, Lawrence Berkeley National Laboratory, Berkeley, CA 94720

11
12 *Correspondence to:* Brian J. Majestic (brian.majestic@du.edu)

13
14 Abstract

15
16 Iron is the most abundant transition element in airborne PM, primarily existing as Fe(II)
17 or Fe(III). Generally, the fraction of water-soluble iron is greater in urban areas compared to
18 areas dominated by crustal emissions. To better understand the origin of water-soluble iron in
19 urban areas, tail-pipe emission samples were collected from 32 vehicles with emission
20 certifications of Tier 0, low emission vehicles (LEV I), tier two low emission vehicles (LEV II),
21 ultralow emission vehicles (ULEV), superultra-low emission vehicles (SULEV), and partial-zero
22 emission vehicles (PZEV). Components quantified included gases, inorganic ions, elemental
23 carbon (EC), organic carbon (OC), total metals and water-soluble metals. Naphthalene and
24 intermediate volatility organic compounds (IVOC) were quantified for a subset of vehicles. The
25 IVOC quantified contained 12 to 18 carbons and were divided into three subgroups: aliphatic,
26 single ring aromatic (SRA), and polar (material not classified as either aliphatic or SRA). Iron
27 solubility in the tested vehicles ranged from 0 – 82% (average = 30%). X-ray absorption near
28 edge structure (XANES) spectroscopy showed that Fe(III) was the primary oxidation state in 14
29 of the 16 tested vehicles, confirming that the presence of Fe(II) was not the main driver of water-
30 soluble Fe. Correlation of water-soluble iron to sulfate was insignificant, as was correlation to

31 every chemical component, except to naphthalene and some C12- C18 IVOCs with R^2 values as
32 high as 0.56. A controlled benchtop study confirmed that naphthalene, alone, increases iron
33 solubility from soils by a factor of 5.5 and that oxidized naphthalene species are created in the
34 extract solution. These results suggest that the large driver in water-soluble iron from primary
35 vehicle tail-pipe emissions is related to the organic composition of the PM. We hypothesize that,
36 during the extraction process, specific components of the organic fraction of the PM are oxidized
37 and chelate the iron into water.

38 1. Introduction

39 Iron has been identified as a limiting nutrient for phytoplankton in approximately half of
40 the world's oceans, with deposition from the atmosphere as the major source (Moore and Abbott,
41 2002; Sholkovitz et al., 2012). Phytoplankton is one of the controlling factors of fixed nitrogen in
42 many parts of the oceans and, consequently, plays a major role in the ocean's biogeochemical
43 cycles (Baker et al., 2006; Chen and Siefert, 2004; Kraemer, 2004; Shi et al., 2012; Tagliabue et
44 al., 2017). Also, water-soluble iron fractions are linked to the creation of reactive oxygen species
45 (ROS) in lung fluid and in environmental matrices through Fenton chemistry (Hamad et al.,
46 2016). These ROS impart oxidative stress on the respiratory system, contributing to various
47 health effects (Landreman et al., 2008; Park et al., 2006; Verma et al., 2014).

48 Annually, approximately 55 Tg of iron enters the atmosphere from crustal sources (Luo
49 et al., 2008). Of this, 14-16 Tg are deposited into the ocean, impacting the marine life and
50 influencing the ecosystems (Gao, 2003; Jickells et al., 2005). Typically, airborne iron from
51 crustal sources ranges from 0.05-2% water-soluble of the total iron (Bonnet, 2004; Sholkovitz et
52 al., 2012). Relative water-soluble iron in urban environments is higher, ranging from 2-50% of
53 the total (Majestic et al., 2007; Sedwick et al., 2007; Sholkovitz et al., 2012). It is suggested that

54 combustion sources including fossil fuel burning, incinerator use and biomass burning may be a
55 large contributor to the water-soluble iron fraction, contributing 0.66-1.07 Tg a⁻¹ of water-soluble
56 iron and this iron has been correlated to anthropogenic sources (Chuang et al., 2005; Luo et al.,
57 2008; Sholkovitz et al., 2009). From these combustion sources, it has been shown that the
58 species of iron differed greatly and had an impact in iron solubility (Fu et al., 2012). Even though
59 total iron emissions from combustion sources are small in comparison to crustal sources, the
60 relative insolubility of crustal iron leads to the possibility that combustion sources contribute
61 20%-100% of water-soluble iron into the atmosphere (Luo et al., 2008; Sholkovitz et al., 2012).

62 Previous studies in tunnels and parking structures have reported iron ranging from five to
63 approximately 3,500 ng m⁻³, revealing that brake wear, tire wear, resuspended road dust, and tail
64 pipe emissions can be important sources of trace elements (Kuang et al., 2017; Lawrence et al.,
65 2013; Li and Xiang, 2013; Lough et al., 2005; Park et al., 2006; Verma et al., 2014). Iron is
66 contained in many fuels which has pre-combusted concentrations ranging from 13-1000 µg L⁻¹
67 (Lee and Von Lehmden, 1973; Santos et al., 2011; Teixeira et al., 2007). Within the engine,
68 computational models of combustion in engines suggest that iron emissions could also originate
69 from the fuel injector nozzle inside the engine block (Liati et al., 2015).

70 There are many different factors that may contribute to water-soluble iron and, as a result,
71 several different hypotheses have been developed relating to how iron is solubilized in ambient
72 atmospheres. First, correlation of ambient iron to sulfates in ambient aerosols suggest the
73 possibility of iron solubilization (Desboeufs et al., 1999; Hand et al., 2004; Mackie et al., 2005;
74 Oakes et al., 2012b). However, laboratory studies investigating the heterogeneous chemistry of
75 iron have not shown any change in iron water-solubility, speciation, or oxidation state upon
76 exposure to gaseous SO₂ (Cartledge et al., 2015; Luo et al., 2005; Majestic et al., 2007; Oakes et

77 al., 2012a). A second hypothesis is that particle-bound iron oxidation state may control iron
78 water solubility. Thus far, the limited field studies have been unable to show that iron oxidation
79 state is correlated to iron's resulting water solubility, as the majority of iron found in aerosol
80 particles is in the less soluble Fe(III) oxidation state (Luo et al., 2005; Majestic et al., 2007;
81 Oakes et al., 2012a). A third, broad, iron solubilization hypothesis emphasizes an iron-organic
82 interaction (Baba et al., 2015; Vile et al., 1987). For example, a significant increase in water-
83 soluble iron is observed in the presence of oxalate and formate in ambient aerosols and in cloud
84 droplets (Paris et al., 2011; Zhu et al., 1993). Even when compared to sulfuric acid, oxalic acid
85 results in a greater increase in iron solubility because of the organic iron interaction (Chen and
86 Grassian, 2013). Other studies have suggested that the photolysis of polycyclic aromatic
87 hydrocarbons leads to reduced iron, which may result in greater iron water solubility (Faiola et
88 al., 2011; Haynes and Majestic, 2019; Haynes et al., 2019; Pehkonen et al., 1993; Zhu et al.,
89 1993). Vehicle exhaust contains many organic species including secondary organic aerosol
90 (SOA) Single-ring aromatic compounds (C6-C9) PAHs, hopanes, steranes, alkanes, organic
91 acids and intermediate volatility organic compound (IVOCs) which are longer chain organic
92 species (Cheung et al., 2010; Zhao et al., 2016).

93 In this study, we explore all three hypotheses (bulk ions, iron oxidation state, and organic
94 speciation) in relation to iron solubility. Specifically, we examine the water-soluble iron emitted
95 from 32 light duty gasoline vehicles with certifications of Tier 0, low emission vehicle (LEV I),
96 tier two low emission vehicles (LEV II), ultralow emission vehicles (ULEV), superultra-low
97 emission vehicles (SULEV), and partial-zero emission vehicles (PZEV). The total and water-
98 soluble trace elements are compared to the ions, gaseous compounds, and organic emissions
99 from the same vehicle set. Additionally, we acquired data on the emitted iron oxidation states on

100 the exhaust particles. From this data set, real tail-pipe emission samples were explored to
101 discover how various components of automobile exhaust affect the water solubility of iron.

102 2. Materials and Methods

103 2.1. Sample Collection

104 Exhaust samples from 32 gasoline vehicles were collected at the California Air Resources
105 Board (CARB) Haagen-Smit laboratory over a six-week period. Standard emission test results
106 from this campaign have been reported previously (Saliba et al., 2017). A description of the
107 dynamometer, emission dilution system, and instrumentation used in the vehicle set up is
108 provided elsewhere (May et al., 2014; Saliba et al., 2017). Briefly, each vehicle was tested on a
109 dynamometer using the cold-start Unified California (UC) Drive Cycle or the hot start Modal
110 Arterial Cycle 4. Emission samples were collected using a constant volume sampler from which
111 a slipstream of dilute exhaust was drawn at a flow rate of 47 L min⁻¹. Particle phase emissions
112 were collected using three sampling trains operated in parallel off of the end of the CVS dilution
113 tunnel. Train 1 contained a Teflon filter (47 mm, Pall-Gelman, Teflo R2PJ047). Train 2
114 contained two quartz filters (47 mm, Pall-Gelman, Tissuquartz 2500 QAOUP) in series. Train 3
115 contained an acid-cleaned Teflon filter followed by a quartz filter (47 mm, Teflo, Pall Life
116 Sciences, Ann Arbor, MI) and the flow rate was 0.5 L min⁻¹ through each Tenax tube. The
117 particulate exhaust emissions were then collected on the pre-cleaned Teflon filters. The Teflon
118 filters were stored in a freezer until extraction and analysis was performed. Filter holders were
119 maintained at 47°C during sampling as per the CFR86 protocol.

120 The vehicles were recruited from private citizens, rental car agencies, or part of the Air
121 Resource Board fleet. The vehicles tested were categorized by model years (1990-2014), vehicle
122 type (passenger car and light-duty trucks), engine technologies (GDI and PFI), emission

123 certification standers (Tier1 to SULEV), make, and model. All vehicles were tested using the
124 same commercial gasoline fuel which had a 10 % ethanol blend and a carbon fraction of 0.82
125 (Saliba et al., 2017).

126 Gases (CO, CO₂, CH₄, NO, and NO₂) and total hydrocarbons (THC) were collected into
127 heated Tedlar bags by UC Drive Cycles. Analysis of CO and CO₂ was measured by
128 nondispersive infrared detectors (IRD-4000), CH₄ by gas chromatography, with detection by a
129 flame ionization detector (FID), NO_x by chemiluminescence (CLD 4000) and THC by FID
130 (Drozd et al., 2016; Saliba et al., 2017). The Teflon filter in Train 1 was analyzed by ion
131 chromatography for water-soluble anions and cations and procedure for these data presented
132 elsewhere (Hickox et al., 2000). Train 2 included two parallel sets of Tenax-TA sorbent tubes
133 (Gerstel) downstream of the Teflon filter. The first set was 2 tubes connected in parallel. One of
134 these tubes was used to collect emissions during the cold start phase of UC (the first five
135 minutes, commonly referred to as bag 1). The other tube was used to sample emissions during
136 the combined hot-running and hot start phases of the UC (bags 1 and 2). The second set of
137 sorbent tubes was connected in series to collect emissions over the entire UC test. The Teflo
138 filter in Train 3 was used for total and water-soluble trace element analysis and particle-bound
139 iron oxidation state and is the focus of this study.

140 2.2. Materials Preparation

141 All vessel cleaning and analytical preparation for the trace elements was performed under
142 a laminar flow hood with incoming air passing through a high efficiency particulate air (HEPA)
143 filter. All water used was purified to 18.2 MΩ-cm (Milli-Q Thermo-Fisher Nanopore). Fifteen
144 and 50 mL plastic centrifuge vials, Petri dishes (Fisher), Teflon forceps (Fisher), syringe
145 (Fisher), nitro cellulose paper (Fisher), and syringe cases (Life Sciences Products) were prepped

146 by an acid cleaning process. For the plastic centrifuge vials, Petri dishes, Teflon forceps, syringe,
147 and syringe cases this involved 24-hour soaks in a 10% reagent grade nitric acid bath followed
148 by 10% reagent grade hydrochloric bath then a 3% trace metal grade nitric acid (Fisher) resting
149 bath with MQ rinses before, after and between each step. The nitro cellulose paper was cleaned
150 by soaking in 2% HCl for 24 hours then rinsing with MQ water. Then, 2% HCl and MQ water
151 were pushed through the filter. Teflon beaker liners were cleaned by an acetone rinse, then an
152 overnight bath of 100% HPLC-grade acetonitrile and a final overnight bath of 5% trace-metal
153 grade nitric acid. 0.20 micron syringe filters (Whatman, Marlborough, MA) were prepared with
154 10% trace-metal grade hydrochloric acid, MQ water and 5% nitric acid rinse.

155 The 47 mm Teflon filters were cleaned by submerging them in 10% trace metal grade
156 nitric acid and rinsing with MQ water. The filters were then stored in the acid cleaned Petri
157 dishes and sealed with Teflon tape for storage.

158 2.3. Water-soluble metals sample preparations

159 Water-soluble elements were extracted for 2 hours from the Teflon filter on a shaker table
160 in 10 mL of MQ water. The water extract was filtered with 2 μ m pore size nitro cellulose filters.
161 The Teflon filter and the nitro cellulose filters were saved for total metals digestion. The water-
162 soluble element extract was acidified to 5% trace-metal grade nitric acid and 2.5% trace-metal
163 grade hydrochloric acid to be analyzed by inductively coupled plasma mass spectrometry (ICP-
164 MS, Agilent 7700).

165 2.4. Sample preparation for total elemental analysis

166 After the polymethylpentene ring was removed from the Teflon filters and ~3% of the
167 filters were measured and cut using a ceramic blade and saved for X-ray absorption near edge

168 structure (XANES) spectroscopy, then the water-soluble elements were extracted, and lastly the
169 polymethylpentene ring was removed from the Teflon filters. The Teflon and the nitro cellulose
170 filters for each sample were placed together into a microwave digestion vessel. To each digestion
171 vessel, 750 μL of concentrated trace metal grade nitric acid, 250 μL of concentrated trace grade
172 hydrochloric acid, 100 μL of concentrated trace grade hydrofluoric acid, and 100 μL of 30%
173 hydrogen peroxide was added. These samples were digested (Ethos EZ, Milestone Inc) according
174 to the following a temperature program: 15-minute ramp to 200 $^{\circ}\text{C}$, then held at 200 $^{\circ}\text{C}$ for 15
175 minutes, and a 60-minute cooling period.(Cartledge and Majestic, 2015) The samples were
176 cooled to room temperature for 1 hour and the solution was diluted to 15 mL with MQ water and
177 analyzed via ICP-MS.

178 2.5. Elemental analysis

179 Blank filters and standard reference materials (SRMs) were digested alongside the
180 exhaust samples using the same digestion process described above. Three SRMs were used to
181 address the recoveries of our digestion process: urban particulate matter (1648a, NIST), San
182 Joaquin Soil (2709a, NIST), and Recycled Auto Catalyst (2556, NIST). The recoveries of the
183 SRMs were between 80-120%. The elements analyzed included Na, Mg, Al, K, Ca, Ti, V, Cr,
184 Mn, Fe, Co, Ni, Cu, Zn, As, Se, Rb, Sr, Mo, Rh, Pd, Ag, Cd, Sb, Cs, Ba, Ce, Pt, Pb, U. Indium
185 (~ 1 ppb) was used as an internal standard and a He collision cell was used to remove isobaric
186 interferences.

187 2.6. XANES Spectroscopy

188 X-ray absorption near-edge structure (XANES) and micro X-ray fluorescence (μXRF)
189 data for 16 vehicle exhaust samples were collected at the Advanced Light Source Microprobe

190 beamline (10.3.2), Lawrence Berkeley National Laboratory, Berkeley, CA (Marcus et al., 2004).
191 To locate iron spots on the filters, a broad μ XRF elemental map of each sample was acquired at
192 10 keV using 12 μ m by 12 μ m pixel size and 50 ms dwell time per pixel. μ XRF spectra were
193 simultaneously recorded on each pixel of the map. Iron oxidation state and iron-bearing phases
194 were investigated using iron K-edge extended XANES. The spectra were recorded in
195 fluorescence mode by continuously scanning the Si (111) monochromator (Quick XAS mode)
196 from 7011 to 7415 eV. The data were calibrated using an iron foil with first derivative set at
197 7110.75 eV (Kraft et al., 1996). All data were recorded using a seven-element solid state Ge
198 detector (Canberra, ON). The spectra were deadtime corrected, deglitched, calibrated, pre-edge
199 background subtracted and post-edge normalized using a suite of LabVIEW custom programs
200 available at the beamline (Marcus et al., 2008). To rapidly survey iron oxidation state, a valence
201 scatter plot was generated from normalized XANES data using a custom Matlab code and a large
202 database of iron standards (10.3.2 XAS database) (Marcus et al., 2008). Least-square linear
203 combination fitting (LCF) was subsequently performed in the range 7090 to 7365 eV to confirm
204 iron valence and further identify the major mineral groups present. The best fit was chosen based
205 on 1) minimum normalized sum-square value ($NSS=100 \times [\sum(\mu_{\text{exp}} - \mu_{\text{fit}})^2 / \sum(\mu_{\text{exp}})^2]$), where the
206 addition of a spectral component to the fit required a 10% or greater improvement in the NSS
207 value, and 2) on the elements detected in the μ XRF spectrum recorded on each XANES spot.
208 The uncertainty on the percentages of species present is estimated to be $\pm 10\%$.

209 2.7. Organic Speciation

210 A subset (10) of the 32 samples were quantified for IVOC using electron impact ionization
211 with methods similar to that of Zhao et al., except adapted for GCxGC methods (Zhao et al.,
212 2015, 2016). IVOC material was classified into three categories: aliphatic, single ring aromatic

213 (SRA), and polar (Drozd et al., 2019). Classification within these three classes of compounds
214 was determined by differences in second dimension retention time (polarity space) and by mass
215 spectral characteristics in our GCxGC-MS analysis. All three classes of compounds were
216 quantified by either compound specific calibration using known standards or relating total ion
217 chromatogram (TIC) signals to calibration standards of similar volatility and polarity. In
218 GCxGC, the TIC signal corresponds to a blob, or a region in volatility and polarity retention
219 space. The GC-Image software package was used to create blobs from 2D chromatograms.
220 Compounds were quantified by relating their TIC signal to that of the nearest standard in terms
221 of polarity and volatility. Volatility bins were defined that are evenly spaced with their center
222 elution times corresponding to each *n*-alkane. TIC blobs were quantified using the calibration for
223 the available standard of similar polarity in the same volatility bin.

224 2.8. Emission Factor Calculations

225 Emissions data are presented as fuel-based emission factors (EF). Emission factors are
226 calculated as the amount of analyte emitted by mass per gram of fuel emitted.

$$227 \quad EF_i(g\ g - fuel^{-1}) = \Delta m_i \frac{x_c(g)}{\Delta CO_2(g) + \Delta CO(g) + \Delta THC(g)}$$

228 ΔCO_2 , ΔCO , and ΔTHC are the background corrected carbon concentration of CO_2 , CO , and
229 THC (Drozd et al., 2016; Goldstein et al., 2017), respectively. x_c is the fuel carbon mass
230 fraction of 0.82. Δm_i is the blank subtracted concentrations of species *i*.

231 2.9. Naphthalene and Iron Benchtop Study

232 To better understand the production of soluble iron during the water extraction process, a
233 bench-top study was performed using three varying forms of iron with naphthalene. The iron

234 stock solutions/suspensions included: 1) standardized San Joaquin soil (NIST SRM 2709a)
235 containing 25 ppm total iron (soluble + insoluble) iron to determine the effects of crustal iron, 2)
236 iron(II) sulfate to a concentration of 25 ppm to examine the effect of a soluble iron(II) source,
237 and 3) iron(III) sulfate to examine a source of soluble iron(III). In parallel, 100 mg of
238 naphthalene crystals were added to 200 mL of MQ water. For the experiment, 99 mL of the
239 naphthalene suspension and 1 mL of the iron suspension were added to Teflon liners (250 ppb
240 iron total), which were inserted into a jacked glass beaker temperature controlled to 25 °C. After
241 16 hr of stirring, 2 ml were filtered (0.2 μm) and acidified to 5% nitric acid. Soluble iron released
242 from the soil both in the presence and absence of naphthalene was analyzed by ICP-MS.
243 Chemical changes in naphthalene in the presence and absence of iron were monitored by HPLC.

244 3. Results and Discussion

245 *3.1. Total and water-soluble element exhaust concentrations*

246 **Table 1:**

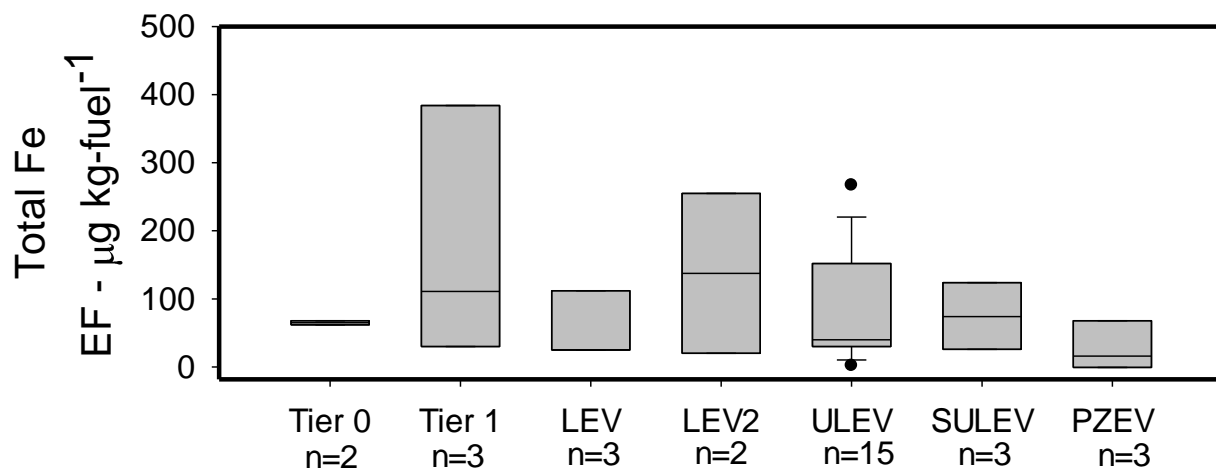
247 Emissions of ions, organic species, gaseous species, and EC/OC from these tests have
248 been published previously (Drozd et al., 2016, 2019; Goldstein et al., 2017; Saliba et al., 2017).
249 In order to obtain a better understanding of the factors that influence iron solubility, we compare
250 these with the total elements, trace elements, and iron oxidation state measurements. Generally,
251 the elements with the highest EF are the lighter crustal elements Ca, Al, and Fe, with average EF
252 200, 100, and 80 μg kg-fuel⁻¹ (Table 1), respectively. Iron has the third highest average EF of all
253 the elements and the highest of all transition elements, ranging from 0 – 200 μg Fe kg-fuel⁻¹.
254 This is followed by three first row transition elements: Zn, Cu, and Ni with the respective
255 average EF of 60, 20, and 5 μg kg-fuel⁻¹. Other notable elements include Rh, Pd and Pt, likely

256 originating from the catalytic convertor, with the respective average EF of 0.05, 0.7, and 0.04 μg
257 kg-fuel^{-1} . Toxic elements include Chromium, Lead, Molybdenum and Antimony with respective
258 EF 5, 0.8, 5 and 0.2 $\mu\text{g kg-fuel}^{-1}$. A previous study has shown that various elements are enriched
259 in used motor oil such as copper, zinc, manganese, iron and lead which could originate from
260 engine wear (Majestic et al., 2009).

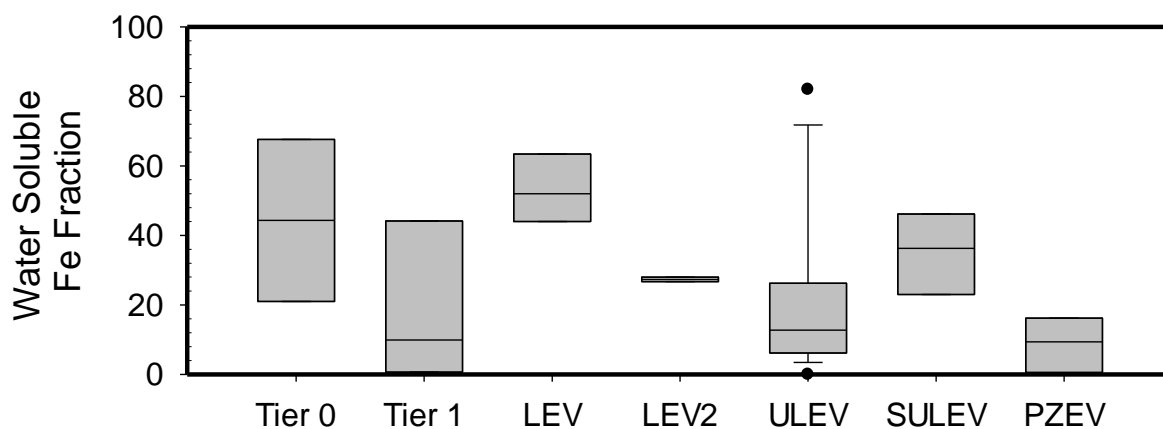
261 Table 1 also shows the EF for the water-soluble fraction of the trace elements. The water-
262 soluble EF for iron ranges from 0-150 $\mu\text{g kg-fuel}^{-1}$; or 0-82% of the total. At 20 $\mu\text{g kg-fuel}^{-1}$,
263 average water-soluble iron was the third largest EF of all elements. There were relatively high
264 emissions of a few other water-soluble elements such as Ca with an average EF of 200 $\mu\text{g kg-}$
265 fuel^{-1} and Zn with tailpipe emissions averaging 40 $\mu\text{g kg-fuel}^{-1}$.

266 **Table 2:**

267 Only a few studies report tailpipe emissions (i.e., dynamometer testing) of trace elements
268 for diesel and gasoline-powered passenger cars and even fewer which have reported iron water
269 Table 2 compares the average exhaust PM composition and trace elements in distance-based
270 emission factors in this study to literature values for other passenger vehicles, including one
271 diesel and three gasoline exhaust studies. For all elements, the distance-based emission factors
272 were greater in the diesel cohort, relative to the gasoline vehicles. Compared to previous studies,
273 the trace elements emitted from older gasoline passenger vehicles resulted in an order of
274 magnitude higher emissions for all elements, except for aluminum, which only showed a factor
275 of ~2 increase in older vehicles (Table 2). Iron shows a large range in the three studies of
276 gasoline vehicles, ranging from 8.3-280 $\mu\text{g km}^{-1}$, compared to the 0-62 $\mu\text{g km}^{-1}$ measured in this
277 study.



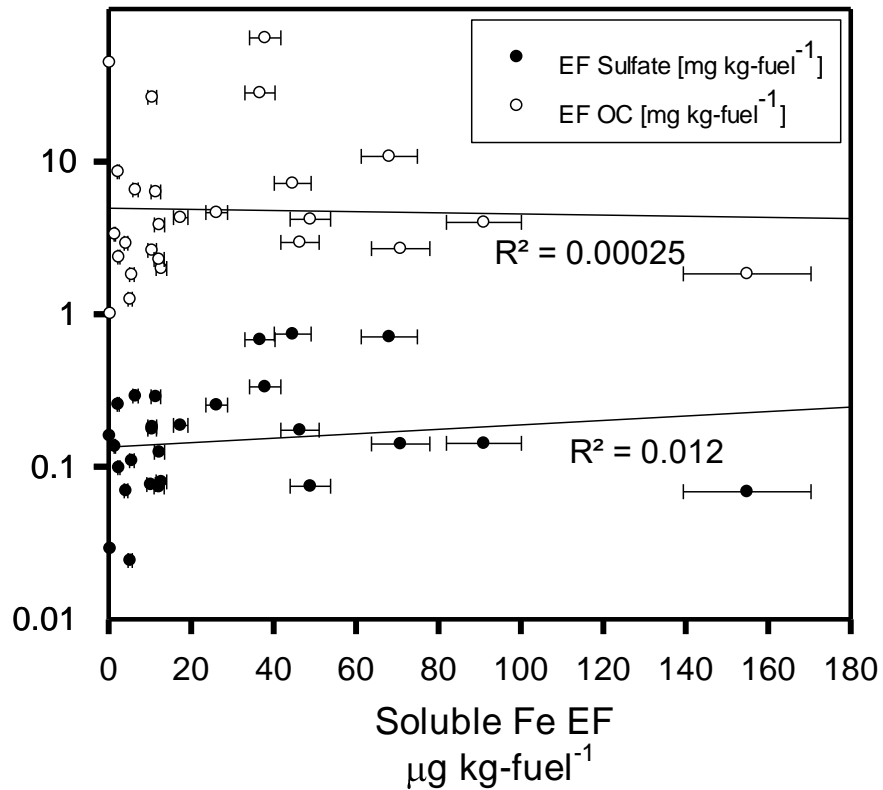
278
 279 Figure 1: Total iron from the 32 vehicles tested reported in EF ($\mu\text{g kg-fuel}^{-1}$). The center black
 280 line represents the median value and the edges of the boxes represent the 25th and 75th percentiles
 281 while the whiskers extent are the 10th and 90th percentiles.



282
 283 Figure 2: Water-soluble iron from the 32 vehicles tested reported in water-soluble iron fraction.
 284 The center black line represents the median value and the edges of the boxes represent the 25th
 285 and 75th percentiles while the whiskers are the 10th and 90th percentiles.

286 The large ranges in iron solubility of the previous studies led us to explore and compare
287 the newer emission certification standard (Figure 1 and 2). Total iron did not trend strongly with
288 emission certification standard, although, on average, total iron is less in the Tier 0 and LEV
289 vehicles. Water-soluble iron shows a small average decrease of approximately $5 \mu\text{g kg-fuel}^{-1}$
290 between ULEV and SULEV vehicles, and a further average decrease for the PZEV vehicles of
291 $3.9 \mu\text{g kg-fuel}^{-1}$.

292 *3.2. Iron correlations with bulk exhaust components and iron oxidation state*

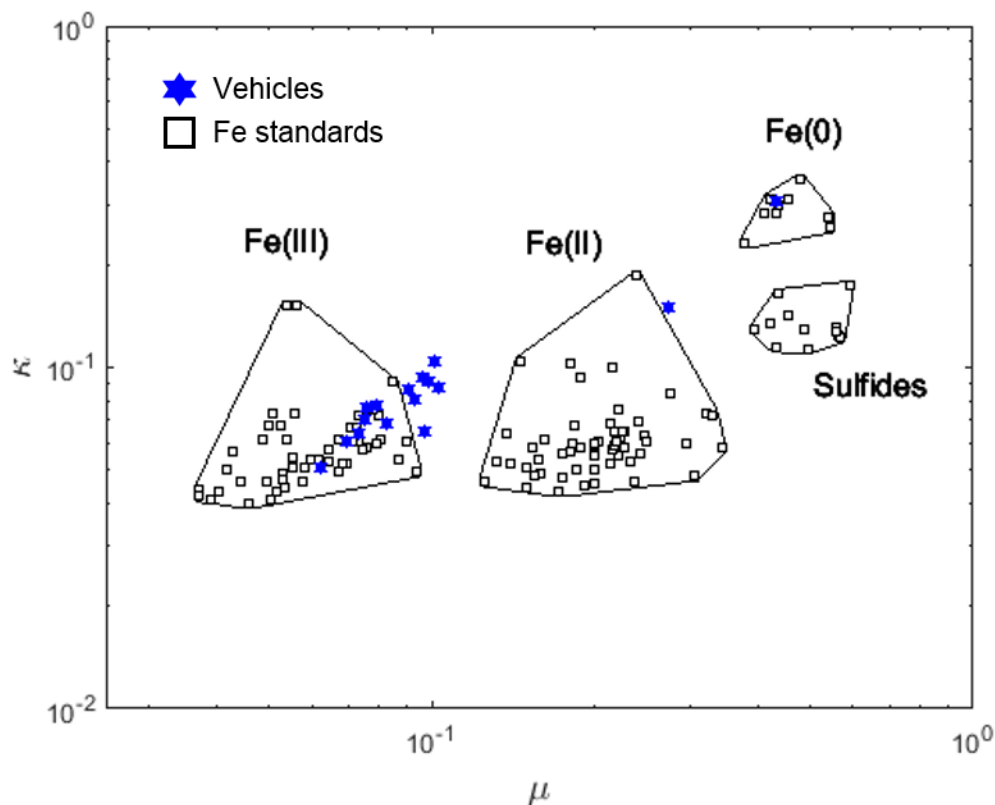


293

294 Figure 3: Linear correlation plots representing EF in mg kg-fuel⁻¹ for sulfate and organic carbon
295 (OC) in μg kg-fuel⁻¹ for water-soluble iron. Correlation lines and R² values for all elements are
296 shown.

297

298 To explore what factors and if any exhaust components are associated with the presence
299 of water-soluble iron, linear regression analyses were used to compare soluble iron to different
300 chemical species in the exhaust. Solubility from the direct exhaust was explored by comparing
301 the EFs of both sulfate and nitrate to iron, and water-soluble iron was not correlated to either of
302 these species (SI1 and Figure 3). The EFs for water-soluble iron and CO₂ showed no correlation,
303 suggesting that overall fuel use was not an important factor for water-soluble iron production
304 (SI1). Total iron was correlated to the water-soluble iron indicating the total amount of iron may
305 have an impact on soluble iron (SI2). Finally, to evaluate if water-soluble iron and overall
306 particulate carbon relate, the EFs for elemental carbon (EC) and organic carbon (OC) were
307 compared to that of soluble iron and, again, no correlation was observed (SI1 and Figure 3).



308

309 Figure 4: Fe valence scatter plot generated from Fe K-edge XANES data where κ and μ are
 310 normalized absorbance values at 7113 eV and 7117.5 eV respectively. Empty black squares
 311 represent Fe standards of known valence while blue-filled stars represent vehicle exhaust
 312 samples.

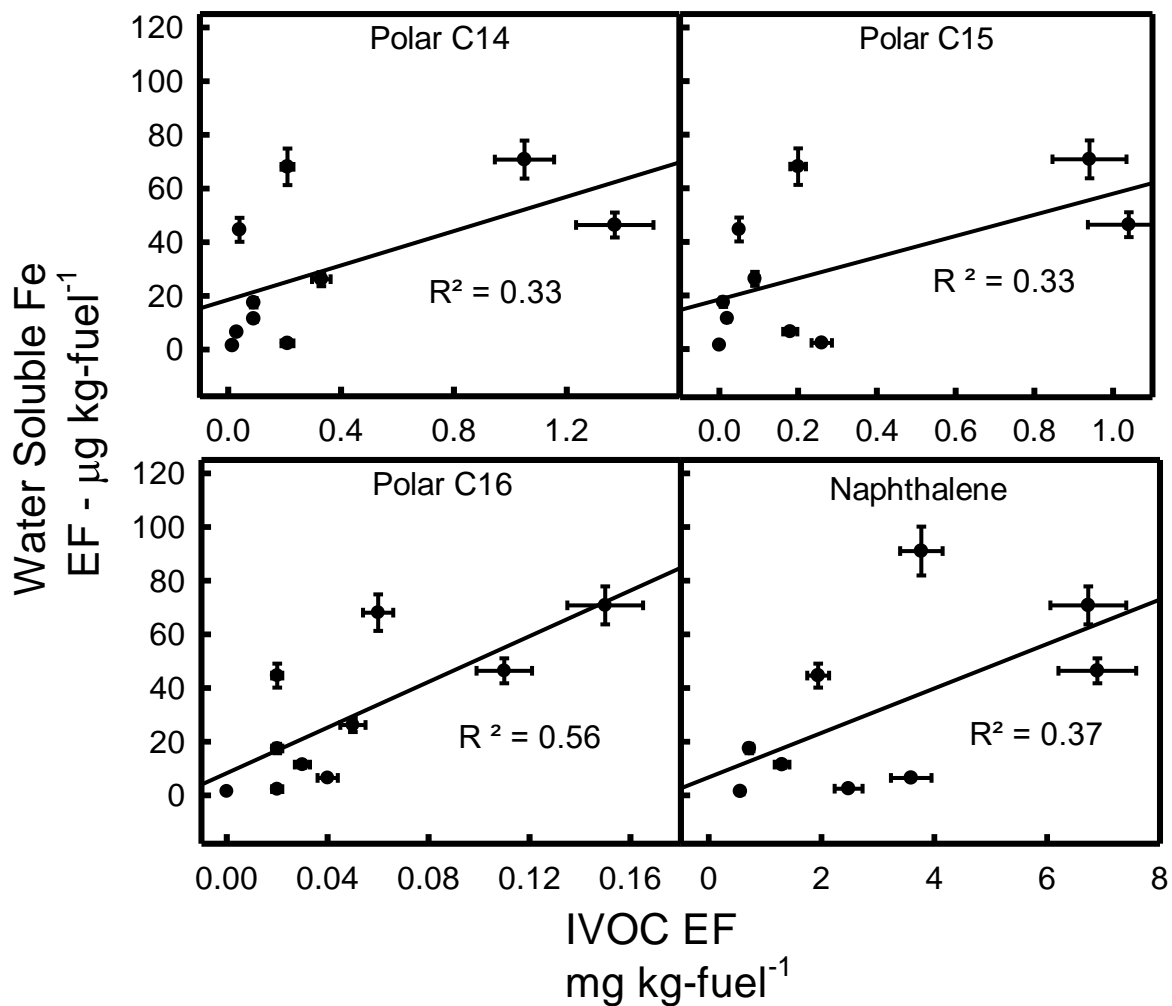
313

314 As no correlation between water-soluble iron and bulk chemical species was observed
 315 (SI1 and SI3), the importance of the particle-bound iron oxidation state was investigated. Since
 316 Fe(II) is known to be more soluble than Fe(III), the expectation was that exhaust samples having
 317 a large Fe(II) character would have a greater iron solubility, relative to those containing Fe(III)
 318 or to Fe(0) (Stumm and Morgan, 1996). Figure 3 presents a scatter plot of the iron valence in 16
 319 of the exhaust samples, compared with iron-bearing standards of known valence. This valence

320 plot is generated from iron K-edge XANES data where parameters κ and μ are defined as
321 normalized absorbance values at 7113 eV and 7117.5 eV, respectively. We observe that the
322 exhaust-iron is primarily in the Fe(III) oxidation state, except for two vehicles: sample 11,
323 dominated by Fe(0) and sample 15, containing a combination of Fe(0) and Fe(III) (SI4). Sample
324 11 is an extreme case, having 0 % iron solubility and highly elevated amount of EC at 305 μg
325 kg-fuel^{-1} (study average = 78 $\mu\text{g kg-Fuel}^{-1}$). The presence of Fe(0) is consistent with high EC, as
326 both observations suggest a lack of oxidation during the combustion and emission process.
327 While the valence plot (Figure 3) put sample 15 as mostly Fe(II), the LCF actually showed that it
328 was a mixture of Fe(0) and Fe(III). And, this sample contained only 10% water-soluble iron, less
329 than the cohort average. The study-wide solid phase iron oxidation state is primarily Fe(III) or
330 mixed oxidation state (Fe(III) and Fe(0)) (see Figure 3), averaging about 30% water-soluble iron,
331 well above the crustal background.

332 LCF XANES fitting (SI4) showed Fe(III) oxides and oxyhydroxides as the dominant group,
333 followed by Fe(III) sulfates and iron silicates (SI4). Hematite ($\alpha\text{-Fe}_2\text{O}_3$) and maghemite ($\gamma\text{-}$
334 Fe_2O_3) were the most consistently detected Fe(III) oxides. Iron was detected in all samples, with
335 Zn, Cr and Cu the main other elements detected in nearly all samples (detection of low-Z
336 elements below sulfur or high-Z elements above zinc was not possible in our experimental
337 conditions). Overall, these results strongly suggest that the main driver of water-soluble iron is
338 not associated with the particle-bound iron oxidation state. Further investigation for the LCF
339 XANES fitting showed that 34% of iron speciated was Fe(III)-oxyhydroxides associated with
340 organic material leading to the investigation of organic species which resulted in a correlation to
341 longer chain IVOC and naphthalene (SI6).

342 *3.3. Iron solubility and speciated organics*



343

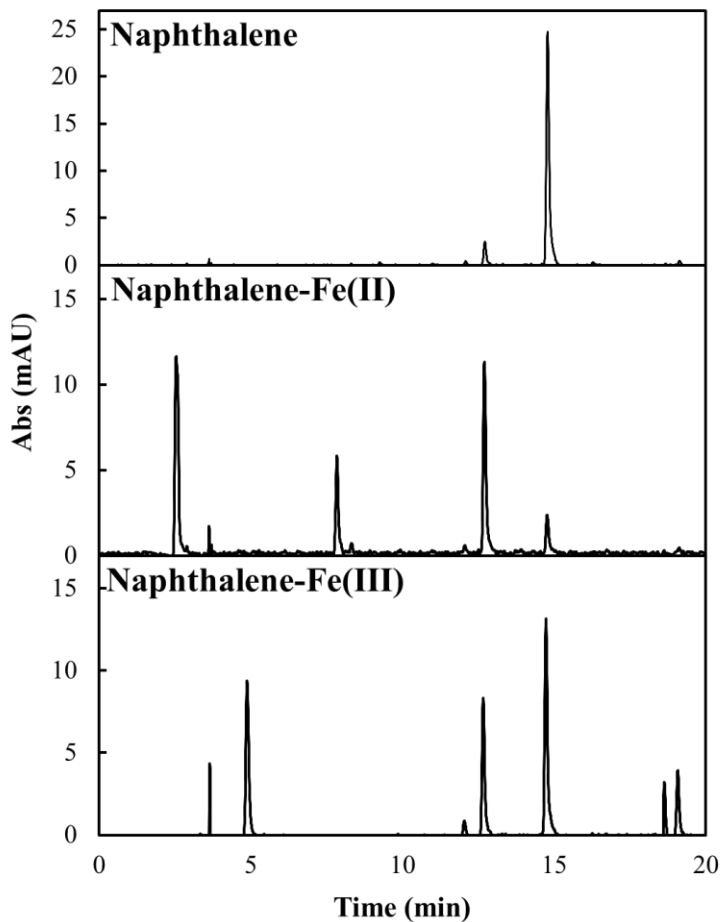
344 Figure 5: Scatter plots of water-soluble iron versus the sum of IVOCs reported in EF (g kg-fuel⁻¹).
 345 1).

346

347 Finally, the relationship between water-soluble iron and speciated organics, specifically
 348 naphthalene and IVOCs, was examined. In contrast with all other measured parameters, Figure 4
 349 shows relatively strong correlations between water-soluble iron and some of the IVOC species.
 350 Figure 4 presents the classifications which have the strongest correlation with water-soluble iron.
 351 Water-soluble iron relationships with other IVOCs can be found in the supplementary

352 information (SI8). The correlation to water-soluble iron is highest for IVOC-polar species with
353 16 carbons ($R^2 = 0.56$). The variance of figure 4 could result from the fact that, in addition to the
354 IVOCs, other factors also influence iron water solubility.

355 As water-soluble iron trends well with naphthalene and polar-IVOCs, but not with bulk
356 EC or OC, it is highly suggestive that iron solubility from the direct emission samples is
357 primarily dependent on interactions with the species of carbon present in the particles during the
358 extraction process. To better understand these interactions, a preliminary laboratory study was
359 conducted to explore both i) the effect of these organic compounds on iron solubility and ii) the
360 effect of soluble iron on the oxidation of organic compounds during the extraction process.
361 Specifically, when naphthalene was added to an insoluble iron source (a soil), iron solubility
362 increased from 0.8 to 4.2 % of the total, or by a factor of ~5.5, showing that the addition of
363 naphthalene, alone, can have a significant effect on iron water solubility and that this effect
364 likely is important during the extraction process.



365

366 Figure 6: HPLC of resulting reaction between naphthalene and water-soluble iron. Phthalic acid
 367 at 12.5 minutes, phthalic anhydride at 7.5 minutes, naphthol at 15 minutes and naphthalene at 20
 368 minutes. The column uses a C18 stationary phase on beads with 80Å pore size.

369 Lacking oxidized functional groups, naphthalene was not expected to chelate iron or to,
 370 otherwise, have the ability to increase iron solubility. Thus, we investigated what compounds are
 371 formed from naphthalene during these extractions. Figure 5 shows the new oxidized products
 372 formed from naphthalene during the water extraction. In the presence of soluble iron, HPLC
 373 retention time analysis shows the presence of phthalic acid (12.5 minutes), phthalic anhydride
 374 (7.5 minutes), and naphthol (15 minutes). The peaks at and below 5 min were not identified but,

375 based on the retention times, these are thought to be low molecular mass, highly polar organic
376 products and is consistent with other studies (Haynes et al., 2019)

377 3.4. Iron-carbon interactions

378 There are at least two methods in which organic compounds can lead to increased iron
379 solubility: a) reduction of Fe(III) to Fe(II) or b) bringing soluble iron into solution via chelation.
380 The first one is generally achieved by photochemistry (Pehkonen et al., 1993), which is not
381 directly applicable to this study. The second, chelation, generally requires oxidized functional
382 groups as shown in Figure 5. The extent of the ability for phthalic acid (a dicarboxylic acid) to
383 chelate iron has not been reported, however, it is known that similar molecular mass organic
384 diacids have significant ability to chelate iron, thus pulling it into solution (Paris and Desboeufs,
385 2013). Here, we suggest that the observed correlations between IVOC/naphthalene and water-
386 soluble iron can be best explained with Fenton reactions, resulting in propagation of radical
387 reactions (Pehkonen et al., 1993). As shown from the Fe XANES valance plot, the iron is
388 predominately Fe(III) (Figure 4). In addition to the Fe(III), it has been shown that H₂O₂ forms in
389 PM_{2.5} water extracts and it been speculated that this formation is from various transition metals
390 and/or quinones found in PM_{2.5} (Wang et al., 2012).



394
395 In the presence of H₂O₂, Fe(III) is known to undergo reaction (1) (Neyens and Baeyens,
396 2003; Pignatello et al., 2006), resulting in the formation of Fe(II) and HO₂ (Pignatello et al.,
397 2006; Rubio-Clemente et al., 2014), which degrades into superoxide, O₂⁻, and H⁺ (2). Superoxide
398 has the ability to oxidize organic compounds, particularly aromatic structures (3) (Lair et al.,

399 2008). The resulting structures of these oxidized compounds typically have two oxygen atoms,
400 which could be arranged in various functional groups (Lair et al., 2008; Rubio-Clemente et al.,
401 2014), also observed from the HPLC chromatograms. Oxidized single ring aromatic structures
402 have a strong affinity to iron and have the ability chelate iron into aqueous solution (Haynes and
403 Majestic, 2019; Hosseini and Madarshahian, 2009). Based on the laboratory studies of
404 naphthalene and soluble-iron presented here, naphthalene and/or IVOC oxidation during the
405 extraction process is the most likely path towards increased iron solubility in primary tailpipe
406 emissions. This overall process suggests that Fe(III) is emitted through car exhaust through
407 interaction with water and organics undergoes a Fenton like reaction and converted to Fe(II) and
408 the iron is chelated by the resulting oxidized organics.

409 4. Conclusions

410 This study shows water-soluble iron is directly formed from vehicle exhaust and not
411 correlated to sulfates. The results show that iron is solubilized in water by specific organic
412 compounds present in automobile exhaust, and that soluble iron is not necessarily dictated by the
413 overall OC content. Thus, the implication is that anthropogenic water-soluble iron is a result of
414 chelation from specific organic compounds, likely their eventual aqueous reaction products.
415 Although the mechanism of these aqueous transformations were not directly measured in this
416 study, based on Fenton chemistry, the primary compounds are expected to be oxidized versions
417 of naphthalene and/or IVOCs (Ledakowicz et al., 1999). Since these oxidation reactions occur
418 fairly quickly (i.e., during the water extraction), further studies are of interest to better
419 understand how these organic compounds interact with iron as it enters atmospheric waters and,
420 also, the photo-chemical interactions between iron and organics.

421

422

423

424 Acknowledgements

425 The authors thank the excellent and dedicated personnel at the California Air Resources
426 Board, especially at the Haagen–Smit Laboratory. This study was funded by National Science
427 Foundation grant numbers 1342599 and 1549166. This research used resources of the Advanced
428 Light Source, which is a DOE Office of Science User Facility under contract no. DE-AC02-
429 05CH11231. Financial support was provided by the California Air Resources Board (Contract
430 #12-318). The California Air Resources Board also provided substantial in-kind support for
431 vehicle procurement, testing, and emissions characterization.

432 Author contribution

433 The sample collection scheme was designed by Allen L. Robinson, Allen H. Goldstein
434 and Brian J. Majestic. Samples were collected by Benton T. Cartledge and Greg T. Drozd.
435 Organic speciation was performed by Greg T. Drozd. Trace elements were quantified by Joseph
436 R. Salazar. Iron speciation was performed by Joseph R. Salazar, Rachel York-Marini and Brian
437 J. Majestic, with the interpretation effort led by Sirine C. Fakra. Bench-top naphthene
438 experiments were performed by John P. Haynes. Data integration was performed by Joseph R.
439 Salazar. The manuscript was prepared by Joseph R. Salazar and Brian J. Majestic.

440

441

442

443

444

445 References

446 Baba, Y., Yatagai, T., Harada, T. and Kawase, Y.: Hydroxyl radical generation in the photo-
447 fenton process: Effects of carboxylic acids on iron redox cycling, *Chem. Eng. J.*, 277, 229–241,
448 doi:10.1016/j.cej.2015.04.103, 2015.

449 Baker, A. R., Jickells, T. D., Witt, M. and Linge, K. L.: Trends in the solubility of iron,
450 aluminium, manganese and phosphorus in aerosol collected over the Atlantic Ocean, *Mar.*
451 *Chem.*, 98(1), 43–58, doi:10.1016/j.marchem.2005.06.004, 2006.

452 Bonnet, S.: Dissolution of atmospheric iron in seawater, *Geophys. Res. Lett.*, 31(3), L03303,
453 doi:10.1029/2003GL018423, 2004.

454 Cartledge, B. T. and Majestic, B. J.: Metal concentrations and soluble iron speciation, *Atmos.*
455 *Pollut. Res.*, (6), 495–505, 2015.

456 Cartledge, B. T., Marcotte, A. R., Herckes, P., Anbar, A. D. and Majestic, B. J.: The Impact of
457 Particle Size, Relative Humidity, and Sulfur Dioxide on Iron Solubility in Simulated
458 Atmospheric Marine Aerosols, *Environ. Sci. Technol.*, 49(12), 7179–7187,
459 doi:10.1021/acs.est.5b02452, 2015.

460 Chen, Y. and Siefert, R. L.: Seasonal and spatial distributions and dry deposition fluxes of
461 atmospheric total and labile iron over the tropical and subtropical North Atlantic Ocean, *J.*
462 *Geophys. Res. D Atmos.*, 109(9), doi:10.1029/2003JD003958, 2004.

463 Cheung, K. L., Ntziachristos, L., Tzamkiozis, T., Schauer, J. J., Samaras, Z., Moore, K. F. and

464 Sioutas, C.: Emissions of particulate trace elements, metals and organic species from gasoline,
465 diesel, and biodiesel passenger vehicles and their relation to oxidative potential, *Aerosol Sci.*
466 *Technol.*, 44(7), 500–513, doi:10.1080/02786821003758294, 2010.

467 Chuang, P. Y., Duvall, R. M., Shafer, M. M. and Schauer, J. J.: The origin of water soluble
468 particulate iron in the Asian atmospheric outflow, *Geophys. Res. Lett.*, 32(7), 1–4,
469 doi:10.1029/2004GL021946, 2005.

470 Desboeufs, K. V, Losno, R. and Cholbi, S.: The pH-dependent dissolution of wind-transported, ,
471 104, 1999.

472 Drozd, G. T., Zhao, Y., Saliba, G., Frodin, B., Maddox, C., Weber, R. J., Chang, M. C. O.,
473 Maldonado, H., Sardar, S., Robinson, A. L. and Goldstein, A. H.: Time Resolved Measurements
474 of Speciated Tailpipe Emissions from Motor Vehicles: Trends with Emission Control
475 Technology, Cold Start Effects, and Speciation, *Environ. Sci. Technol.*, 50(24), 13592–13599,
476 doi:10.1021/acs.est.6b04513, 2016.

477 Drozd, G. T., Zhao, Y., Saliba, G., Frodie, B., Maddox, C., Chang, M.-C. O., Maldonado, H.,
478 Sardar, S., Weber, R. J., Robinson, A. L. and Goldstein, A. H.: Detailed Speciation of
479 Intermediate Volatility and Semivolatile Organic Compound Emissions from Gasoline Vehicles:
480 Effects of Cold-Starts and Implications for Secondary Organic Aerosol Formation., *Environ. Sci.*
481 *Technol.*, 53(3), 1706–1714, 2019.

482 Faiola, C., Johansen, A. M., Rybka, S., Nieber, A., Thomas, C., Bryner, S., Johnston, J.,
483 Engelhard, M., Nachimuthu, P. and Owens, K. S.: Ultrafine particulate ferrous iron and
484 anthracene associations with mitochondrial dysfunction, *Aerosol Sci. Technol.*, 45(9), 1109–
485 1122, doi:10.1080/02786826.2011.581255, 2011.

486 Gao, Y.: Aeolian iron input to the ocean through precipitation scavenging: A modeling
487 perspective and its implication for natural iron fertilization in the ocean, *J. Geophys. Res.*,
488 108(D7), 4221, doi:10.1029/2002JD002420, 2003.

489 Goldstein, A., Robinson, A., Kroll, J., Drozd, G., Zhao, Y., Saliba, G., Saleh, R. and Presto, A.:
490 Investigating Semi-Volatile Organic Compound Emissions from Light-Duty Vehicles., 2017.

491 Hamad, S. H., Schauer, J. J., Antkiewicz, D. S., Shafer, M. M. and Kadhim, A. K. H.: ROS
492 production and gene expression in alveolar macrophages exposed to PM_{2.5} from Baghdad, Iraq:
493 Seasonal trends and impact of chemical composition, *Sci. Total Environ.*, 543, 739–745,
494 doi:10.1016/j.scitotenv.2015.11.065, 2016.

495 Hand, J. L., Mahowald, N. M., Chen, Y., Siefert, R. L., Luo, C., Subramaniam, A. and Fung, I.:
496 Estimates of atmospheric-processed soluble iron from observations and a global mineral aerosol
497 model: Biogeochemical implications, *J. Geophys. Res. D Atmos.*, 109(17), 1–21,
498 doi:10.1029/2004JD004574, 2004.

499 Haynes, J. and Majestic, B.: Role of polycyclic aromatic hydrocarbons on the photo-catalyzed
500 solubilization of simulated soil-bound atmospheric iron, *Atmos. Pollut. Res.*,
501 doi:<https://doi.org/10.1016/j.apr.2019.12.007>, 2019.

502 Haynes, J. P., Miller, K. E. and Majestic, B. J.: Investigation into Photoinduced Auto-Oxidation
503 of Polycyclic 2 Aromatic Hydrocarbons Resulting in Brown Carbon Production, *Environ. Sci.*
504 *Technol.*, 53(3), 10.1021/acs.est.8b05704, doi:10.1021/acs.est.8b05704, 2019.

505 Hickox, W. H., Werner, B. and Gaffney, P.: Air Resources Board, , (Mld), 1–6 [online]
506 Available from: http://www.arb.ca.gov/ei/see/memo_ag_emission_factors.pdf, 2000.

507 Hosseini, M. S. and Madarshahian, S.: Investigation of charge transfer complex formation
508 between Fe(III) and 2,6-Dihydroxy benzoic acid and its applications for spectrophotometric
509 determination of iron in aqueous media, *E-Journal Chem.*, 6(4), 985–992,
510 doi:10.1155/2009/417303, 2009.

511 Jickells, T. D., An, Z. S., Andersen, K. K., Baker, a R., Bergametti, G., Brooks, N., Cao, J. J.,
512 Boyd, P. W., Duce, R. a, Hunter, K. a, Kawahata, H., Kubilay, N., LaRoche, J., Liss, P. S.,
513 Mahowald, N., Prospero, J. M., Ridgwell, a J., Tegen, I. and Torres, R.: Global iron connections
514 between desert dust, ocean biogeochemistry, and climate., *Science*, 308(5718), 67–71,
515 doi:10.1126/science.1105959, 2005.

516 Kraemer, S. M.: Iron oxide dissolution and solubility in the presence of siderophores, *Aquat.*
517 *Sci.*, 66(1), 3–18, doi:10.1007/s00027-003-0690-5, 2004.

518 Kraft, S., Stümpel, J. and Becker, P.: High resolution x-ray absorption spectroscopy with
519 absolute energy calibration for the determination of absorption edge energiestle, *Rev. Sci.*
520 *Instrum.*, 67, 681, 1996.

521 Kuang, X. M., Scott, J. A., da Rocha, G. O., Betha, R., Price, D. J., Russell, L. M., Cocker, D. R.
522 and Paulson, S. E.: Hydroxyl radical formation and soluble trace metal content in particulate
523 matter from renewable diesel and ultra low sulfur diesel in at-sea operations of a research vessel,
524 *Aerosol Sci. Technol.*, 51(2), 147–158, doi:10.1080/02786826.2016.1271938, 2017.

525 Lair, A., Ferronato, C., Chovelon, J. M. and Herrmann, J. M.: Naphthalene degradation in water
526 by heterogeneous photocatalysis: An investigation of the influence of inorganic anions, *J.*
527 *Photochem. Photobiol. A Chem.*, 193(2–3), 193–203, doi:10.1016/j.jphotochem.2007.06.025,
528 2008.

529 Landreman, A. P., Shafer, M. M., Hemming, J. C., Hannigan, M. P. and Schauer, J. J.: A
530 Macrophage-Based Method for the Assessment of the Reactive Oxygen Species (ROS) Activity
531 of Atmospheric Particulate Matter (PM) and Application to Routine (Daily-24 h) Aerosol
532 Monitoring Studies, *Aerosol Sci. Technol.*, 42(11), 946–957, doi:10.1080/02786820802363819,
533 2008.

534 Lawrence, S., Sokhi, R., Ravindra, K., Mao, H., Prain, H. D. and Bull, I. D.: Source
535 apportionment of traffic emissions of particulate matter using tunnel measurements, *Atmos.*
536 *Environ.*, 77, 548–557, doi:10.1016/j.atmosenv.2013.03.040, 2013.

537 Ledakowicz, S., Miller, J. S. and Olejnik, D.: Oxidation of PAHs in water solutions by
538 ultraviolet radiation combined with hydrogen peroxide, *Int. J. Photoenergy*, 1(1), 1–6,
539 doi:10.1155/S1110662X99000100, 1999.

540 Li, Y. and Xiang, R.: Particulate pollution in an underground car park in Wuhan, China,
541 *Particuology*, 11(1), 94–98, doi:10.1016/j.partic.2012.06.010, 2013.

542 Lough, G. C., Schauer, J. J., Park, J. S., Shafer, M. M., Deminter, J. T. and Weinstein, J. P.:
543 Emissions of metals associated with motor vehicle roadways, *Environ. Sci. Technol.*, 39(3), 826–
544 836, doi:10.1021/es048715f, 2005.

545 Luo, C., Mahowald, N. M., Meskhidze, N., Chen, Y., Siefert, R. L., Baker, A. R. and Johansen,
546 A. M.: Estimation of iron solubility from observations and a global aerosol model, *J. Geophys.*
547 *Res. Atmos.*, 110(23), 1–23, doi:10.1029/2005JD006059, 2005.

548 Luo, C., Mahowald, N., Bond, T., Chuang, P. Y., Artaxo, P., Siefert, R., Chen, Y. and Schauer,
549 J.: Combustion iron distribution and deposition, *Global Biogeochem. Cycles*, 22,
550 doi:10.1029/2007GB002964, 2008.

551 Mackie, D. S., Boyd, P. W., Hunter, K. A. and McTainsh, G. H.: Simulating the cloud processing
552 of iron in Australian dust: pH and dust concentration, *Geophys. Res. Lett.*, 32(6), 1–4,
553 doi:10.1029/2004GL022122, 2005.

554 Majestic, B. J., Schauer, J. J. and Shafer, M. M.: Application of synchrotron radiation for
555 measurement of iron red-ox speciation in atmospherically processed aerosols, *Atmos. Chem.*
556 *Phys. Atmos. Chem. Phys.*, 7(Iii), 2475–2487, doi:10.5194/acpd-7-1357-2007, 2007.

557 Majestic, B. J., Anbar, A. D. and Herckes, P.: Elemental and iron isotopic composition of
558 aerosols collected in a parking structure, *Sci. Total Environ.*, 407(18), 5104–5109,
559 doi:10.1016/j.scitotenv.2009.05.053, 2009.

560 Marcus, M. A., Macdowell, A. A., Celestre, R., Manceau, A., Miller, T., Padmore, H. A. and
561 Sublett, R. E.: Beamline 10.3.2 at ALS: a hard X-ray microprobe for environmental and
562 materials sciences, *J. Synchrotron Radiat.*, 11, 239–247, doi:10.1107/S0909049504005837,
563 2004.

564 Marcus, M. A., Westphal, A. J. and Fakra, S. C.: Classification of Fe-bearing species from K-
565 edge XANES data using two-parameter correlation plots, *J. Synchrotron Radiat.*, 15(5), 463–
566 468, doi:10.1107/S0909049508018293, 2008.

567 May, A. A., Nguyen, N. T., Presto, A. A., Gordon, T. D., Lipsky, E. M., Karve, M., Gutierrez,
568 A., Robertson, W. H., Zhang, M., Brandow, C., Chang, O., Chen, S., Cicero-Fernandez, P.,
569 Dinkins, L., Fuentes, M., Huang, S. M., Ling, R., Long, J., Maddox, C., Massetti, J., McCauley,
570 E., Miguel, A., Na, K., Ong, R., Pang, Y., Rieger, P., Sax, T., Truong, T., Vo, T., Chattopadhyay,
571 S., Maldonado, H., Maricq, M. M. and Robinson, A. L.: Gas- and particle-phase primary
572 emissions from in-use, on-road gasoline and diesel vehicles, *Atmos. Environ.*, 88, 247–260,

573 doi:10.1016/j.atmosenv.2014.01.046, 2014.

574 Moore, J. K. and Abbott, M. R.: Surface chlorophyll concentrations in relation to the Antarctic
575 Polar Front: Seasonal and spatial patterns from satellite observations, *J. Mar. Syst.*, 37(1–3), 69–
576 86, doi:10.1016/S0924-7963(02)00196-3, 2002.

577 Neyens, E. and Baeyens, J.: A review of classic Fenton’s peroxidation as an advanced oxidation
578 technique, *J. Hazard. Mater.*, 98(1–3), 33–50, doi:10.1016/S0304-3894(02)00282-0, 2003.

579 Norbeck, J. M., Durbin, T. D. and Truex, T. J.: Measurement of primary particulate matter
580 emissions from light-duty motor vehicles, Riverside., 1998.

581 Oakes, M., Weber, R. J., Lai, B., Russell, A. and Ingall, E. D.: Characterization of iron
582 speciation in urban and rural single particles using XANES spectroscopy and micro X-ray
583 fluorescence measurements: Investigating the relationship between speciation and fractional iron
584 solubility, *Atmos. Chem. Phys.*, 12(2), 745–756, doi:10.5194/acp-12-745-2012, 2012a.

585 Oakes, M., Ingall, E. D., Lai, B., Shafer, M. M., Hays, M. D., Liu, Z. G., Russell, A. G. and
586 Weber, R. J.: Iron solubility related to particle sulfur content in source emission and ambient fine
587 particles, *Environ. Sci. Technol.*, 46(12), 6637–6644, doi:10.1021/es300701c, 2012b.

588 Paris, R. and Desboeufs, K. V.: Effect of atmospheric organic complexation on iron-bearing dust
589 solubility, *Atmos. Chem. Phys.*, 13(9), 4895–4905, doi:10.5194/acp-13-4895-2013, 2013.

590 Paris, R., Desboeufs, K. V. and Journet, E.: Variability of dust iron solubility in atmospheric
591 waters: Investigation of the role of oxalate organic complexation, *Atmos. Environ.*, 45(36),
592 6510–6517, doi:10.1016/j.atmosenv.2011.08.068, 2011.

593 Park, S., Nam, H., Chung, N., Park, J.-D. and Lim, Y.: The role of iron in reactive oxygen

594 species generation from diesel exhaust particles, *Toxicol. Vitr.*, 20(6), 851–857,
595 doi:10.1016/j.tiv.2005.12.004, 2006.

596 Pehkonen, S. O., Siefert, R., Erel, Y., Webb, S. and Hoffmann, M. R.: Photoreduction of Iron
597 Oxyhydroxides in the Presence of Important Atmospheric Organic Compounds, *Environ. Sci.*
598 *Technol.*, 27(10), 2056–2062, doi:10.1021/es00047a010, 1993.

599 Pignatello, J. J., Oliveros, E. and MacKay, A.: Advanced oxidation processes for organic
600 contaminant destruction based on the fenton reaction and related chemistry, *Crit. Rev. Environ.*
601 *Sci. Technol.*, 36(1), 1–84, doi:10.1080/10643380500326564, 2006.

602 Rubio-Clemente, A., Torres-Palma, R. A. and Peñuela, G. A.: Removal of polycyclic aromatic
603 hydrocarbons in aqueous environment by chemical treatments: A review, *Sci. Total Environ.*,
604 478, 201–225, doi:10.1016/j.scitotenv.2013.12.126, 2014.

605 Saliba, G., Saleh, R., Zhao, Y., Presto, A. A., Lambe, A. T., Frodin, B., Sardar, S., Maldonado,
606 H., Maddox, C., May, A. A., Drozd, G. T., Goldstein, A. H., Russell, L. M., Hagen, F. and
607 Robinson, A. L.: Comparison of Gasoline Direct-Injection (GDI) and Port Fuel Injection (PFI)
608 Vehicle Emissions: Emission Certification Standards, Cold-Start, Secondary Organic Aerosol
609 Formation Potential, and Potential Climate Impacts, *Environ. Sci. Technol.*, 51(11), 6542–6552,
610 doi:10.1021/acs.est.6b06509, 2017.

611 Schauer, J. J., Kleeman, M. J., Cass, G. R. and Simoneit, B. R. T.: Measurement of emissions
612 from air pollution sources. 5. C1-C32 organic compounds from gasoline-powered motor
613 vehicles., *Environ. Sci. Technol.*, 36(6), 1169–1180, doi:10.1021/es0108077, 2002.

614 Sedwick, P. N., Sholkovitz, E. R. and Church, T. M.: Impact of anthropogenic combustion
615 emissions on the fractional solubility of aerosol iron: Evidence from the Sargasso Sea,

616 Geochemistry, Geophys. Geosystems, 8(10), doi:10.1029/2007GC001586, 2007.

617 Shi, Z., Krom, M. D., Jickells, T. D., Bonneville, S., Carslaw, K. S., Mihalopoulos, N., Baker, A.
618 R. and Benning, L. G.: Impacts on iron solubility in the mineral dust by processes in the source
619 region and the atmosphere: A review, *Aeolian Res.*, 5, 21–42, doi:10.1016/j.aeolia.2012.03.001,
620 2012.

621 Sholkovitz, E. R., Sedwick, P. N. and Church, T. M.: Influence of anthropogenic combustion
622 emissions on the deposition of soluble aerosol iron to the ocean: Empirical estimates for island
623 sites in the North Atlantic, *Geochim. Cosmochim. Acta*, 73(14), 3981–4003,
624 doi:10.1016/j.gca.2009.04.029, 2009.

625 Sholkovitz, E. R., Sedwick, P. N., Church, T. M., Baker, A. R. and Powell, C. F.: Fractional
626 solubility of aerosol iron: Synthesis of a global-scale data set, *Geochim. Cosmochim. Acta*, 89,
627 173–189, doi:10.1016/j.gca.2012.04.022, 2012.

628 Stumm, W. and Morgan, J. J.: *Aquatic Chemistry: Chemical Equilibria and Rates in Natural*
629 *Waterse*, 3rd ed., Wiley-Interscience., 1996.

630 Tagliabue, A., Bowie, A. R., Philip, W., Buck, K. N., Johnson, K. S. and Saito, M. A.: Review
631 The integral role of iron in ocean biogeochemistry, *Nat. Publ. Gr.*, 543(7643), 51–59,
632 doi:10.1038/nature21058, 2017.

633 Verma, V., Fang, T., Guo, H., King, L., Bates, J. T., Peltier, R. E., Edgerton, E., Russell, A. G.
634 and Weber, R. J.: Reactive oxygen species associated with water-soluble PM_{2.5} in the
635 southeastern United States: Spatiotemporal trends and source apportionment, *Atmos. Chem.*
636 *Phys.*, 14(23), 12915–12930, doi:10.5194/acp-14-12915-2014, 2014.

637 Vile, G. F., Winterbourn, C. C. and Sutton, H. C.: Radical-driven fenton reactions: Studies with
638 paraquat, adriamycin, and anthraquinone 6-sulfonate and citrate, ATP, ADP, and pyrophosphate
639 iron chelates, *Arch. Biochem. Biophys.*, 259(2), 616–626, doi:10.1016/0003-9861(87)90528-5,
640 1987.

641 Wang, Y., Arellanes, C. and Paulson, S. E.: Hydrogen peroxide associated with ambient fine-
642 mode, diesel, and biodiesel aerosol particles in Southern California, *Aerosol Sci. Technol.*, 46(4),
643 394–402, doi:10.1080/02786826.2011.633582, 2012.

644 Zhao, Y., Nguyen, N. T., Presto, A. A., Hennigan, C. J., May, A. A. and Robinson, A. L.:
645 Intermediate Volatility Organic Compound Emissions from On-Road Diesel Vehicles: Chemical
646 Composition, Emission Factors, and Estimated Secondary Organic Aerosol Production, *Env. Sci.*
647 *Tech.*, 49, 11516–11526, doi:10.1021/acs.est.5b02841, 2015.

648 Zhao, Y., Nguyen, N. T., Presto, A. A., Hennigan, C. J., May, A. A. and Robinson, A. L.:
649 Intermediate Volatility Organic Compound Emissions from On-Road Gasoline Vehicles and
650 Small Off-Road Gasoline Engines., *Environ. Sci. Technol.*, 50, 4554–4563,
651 doi:10.1021/acs.est.5b06247, 2016.

652 Zhu, X., Prospero, J. M., Savoie, D. L., Millero, F. J., Zika, R. G. and Saltzman, E. S.:
653 Photoreduction of iron(III) in marine mineral aerosol solutions, *J. Geophys. Res. Atmos.*,
654 98(D5), 9039–9046, doi:10.1029/93JD00202, 1993.

655 Tables and Figures and Captions

656 Table 1: Average of total trace total and water soluble elements from car exhaust reported in EF
657 ($\mu\text{g kg-fuel}^{-1}$). These samples represent a range of different makes and models of cars. The
658 values in the parenthesis are the range of the vehicle population. (n=32)

659 Table 2: Comparison of exhaust composition in g km^{-1} from different dynamometer studies
660 which included both gasoline and diesel powered light duty vehicles. The values are the mean of
661 the vehicle population and the values in the parenthesis are the minimum and maximum values.
662 This table is in g km^{-1} opposed to g kg-fuel^{-1} in Table 1.

663
664
665
666
667
668
669
670
671
672
673
674
675
676

Table 1:

	Total Elements	Water-Soluble Elements
Trace elements ($\mu\text{g kg-fuel}^{-1}$)		
Na	50 (0, 200)	30 (0, 100)
Mg	40 (0, 200)	8 (0, 60)
Al	100 (0, 2000)	20 (0, 100)
K	20 (0, 100)	20 (0, 100)

Ca	200 (0, 1000)	200 (0, 1000)
Ti	1 (0, 60)	0.2 (0, 2)
V	0.02 (0, 0.7)	0.02 (0, 0.7)
Cr	5 (0.04, 20)	0.6 (0, 4)
Mn	2 (0.02, 10)	1 (0.007, 8)
Fe	80 (0, 400)	20 (0, 200)
Co	0.2 (0, 1)	0.04 (0, 0.7)
Ni	5 (0, 30)	2 (0, 10)
Cu	20 (0, 200)	20 (0, 100)
Zn	60 (0, 300)	40 (0, 300)
As	0.006 (0, 0.03)	0.006 (0, 0.03)
Se	0.3 (0, 2)	0.05 (0, 0.5)
Rb	0.2 (0, 0.5)	0.01 (0, 0.1)
Sr	1 (0.01, 4)	0.6 (0.003, 3)
Mo	5 (0, 20)	3 (0.002, 30)
Rh	0.06 (0, 0.5)	0.007 (0, 0.1)
Pd	0.8 (0, 6)	0.3 (0, 4)
Ag	0.1 (0, 2)	0.03 (0, 0.5)
Cd	0.007 (0, 0.3)	0.009 (0, 0.05)
Sb	0.2 (0, 1)	0.1 (0, 0.9)
Cs	0.005 (0, 0.02)	0.002 (0, 0.02)
Ba	5 (0, 20)	3 (0.06, 20)
Ce	4 (0, 40)	0.4 (0, 2)
Pt	0.04 (0, 0.4)	0.01 (0, 0.2)
Pb	0.4 (0, 7)	0.3 (0, 7)
U	0.002 (0, 0.03)	0.002 (0, 0.03)

677

678

679

680

681

682

683 Table 2:

	This study Gasoline (n = 32)	Gasoline(Schauer et al., 2002) (n=9)	Gasoline(Norbeck et al., 1998) (n=40)	Diesel(Norbeck et al., 1998) (n=19)
Fleet Age	1990-2014	1981-1994	1972-1990	1977-1993
PM components (mg km ⁻¹)				
OC	1 (0.06, 10)	3.3 ± 0.21	16 ± 32	150 ± 330
EC	10 (0.06, 100)	0.77 ± 0.023	3.5 ± 4.8	160 ± 100
sulfate	0.02 (0.001, 0.1)	0.08 ± 0.16	0.93 ± 1.9	0.77 ± .93
Trace elements (µg km ⁻¹)				
Ag	0.01 (0, 0.25)	4.5 ± 20	0	0
Al	10 (0, 110)	20 ± 17	19 ± 37	31 ± 75
Ba	0.6 (0, 4.4)	0	0	68 ± 75
Ca	30 (0, 130)	26 ± 8.5	81 ± 120	650 ± 930
Cd	0.00 (0, 0.04)	0	0	0
Co	0.01 (0,0.25)	-	0	0
Cr	0.6 (0.008, 4)	0	0	6.2 ± 12
Cu	3 (0, 27)	0	6.2 ± 6.2	19 ± 31
Fe	10 (0, 62)	8.3 ± 2.3	280 ± 680	830 ± 1000
K	2 (0, 15)	3.0 ± 11.3	0	50 ± 170
Mg	7 (0, 120)	-	25 ± 31	99 ± 200
Mn	0.2 (0.002, 1.3)	0	0	6.2 ± 6.2
Mo	0.5 (0, 3.6)	2.3 ± 6.8	0	6.2 ± 12
Ni	0.6 (0, 5.2)	0	6.2 ± 12	12 ± 18
Pb	0.04 (0, 0.57)	0	25 ± 93	19 ± 62
Sb	0.02 (0, 0.21)	17 ± 39	0	0
Sr	0.1 (0, 0.68)	0.75 ± 2.3	0	0
Zn	7 (0, 37)	14 ± 1.5	110 ± 170	810 ± 1500

684

685

686

687